Mixing twist-bend and ferroelectric nematic liquid crystals

Abinash Barthakur,[1] Bidisha Bag ⬤,[1] Santhegudda Jayaramappa Shivaraja ⬤,[1] Jakub Karcz ⬤,[2]
Przemyslaw Kula ⬤,[2] and Surajit Dhara ⬤[1,*]

[1]*School of Physics, University of Hyderabad, Hyderabad 500046, India*
[2]*Institute of Chemistry, Faculty of Advanced Technologies and Chemistry, Military University of Technology, Warsaw 00-908, Poland*

Twist-bend (N_{tb}) and ferroelectric (N_F) nematic liquid crystals exhibit several novel effects and new physical properties. Here, we report experimental studies on the phase diagram and some physical properties of binary mixtures of CB9CB and RM734 mesogens. Both N-N_{tb} and N-N_F phase transition temperatures and the corresponding enthalpies decrease significantly and, eventually, these transitions disappear at some intermediate compositions, stabilizing wide nematic phase (N). Temperature-dependent birefringence several degrees above the N-N_{tb} phase transition shows strong director tilt fluctuations. The critical range of the fluctuations increases with the nematic range and the critical exponent is consistent with the mean field. The spontaneous polarization of RM734 decreases drastically with the addition of CB9CB mesogen. The temperature dependence of the splay elastic constant of the mixtures' high-temperature nematic (N) phase strikingly differs from that of the pristine CB9CB and RM734 mesogens. The study shows that a small inclusion of either compound has a substantial effect on the phase diagram and physical properties.

I. INTRODUCTION

The discovery of new nematic liquid crystals with nanoscale modulation of director (twist-bend nematic, N_{tb}) [1–8] and spontaneous electric polarization (ferroelectric nematic, N_F) [9–15] has created immense interest. They have lower symmetries than the conventional apolar nematic (N) liquid crystals. The twist-bend phase was discovered in bend-core compounds possessing two rigid rodlike mesogenic units connected by a flexible chain [3]. The ferroelectric nematic was discovered in compounds composed of molecules with very high axial dipole moment [9,11]. Interestingly, both these phases were theoretically predicted much before their experimental discoveries [16,17]. Particularly, the ferroelectric nematic was envisaged more than a century ago by Born [16]. These nematic liquid crystals exhibit several new physical properties which are of great fundamental and practical interest. For example, N_{tb} shows a pseudolayer structure [6] and the bend elastic constant K_{33} in the high-temperature nematic phase is very small [6]. On the other hand K_{11} is unusually small near the N-N_F transition [12]. The nematic twist-bend phase provides a compressional elastic constant and smecticlike rheology [18–20]. The N_F phase shows striking electro-optics and a large spontaneous polarization along the director and giant electrohydromechanical effects [21–25]. Ferroelectric nematic LCs also show several interesting defects [26], polarization patterns [27], and flow in confined channels [28]. This polar fluid phase is promising for many applications due to its low threshold field and very fast switching response time.

Experimental investigation on mixtures of mesogens often leads to new phase transitions and physical properties [9,29,30]. In the applications and technology development perspectives the exploration of mixtures has proven to be very successful in achieving optimized physical properties. Recently some interesting phase diagrams and physical properties have been reported on the mixture of ferroelectric nematic liquid crystals [31–33]. However, no studies have been reported on the miscibility of N_{tb} and N_F mesogens. Hence it is not known how these two phases combine and what the resulting effects are. To address these issues we prepared a binary phase diagram by mixing CB9CB and RM734 mesogens. One of the primary objectives of this investigation was to study the miscibility and also to explore the possibility of stabilizing new phases and physical properties. To characterize the mixtures, we systematically investigated phase transitions and measured several properties such as enthalpies, spontaneous polarization, birefringence, dielectric anisotropy, and splay elastic constant as a function of temperature. Our study reveals that CB9CB and RM734 are not well-compatible mesogens and very small concentrations of either of them have significant effects on the phase diagram as well as on the physical properties.

II. EXPERIMENT

Both liquid crystals $1''$, $7''$-bis(4-cyanobiphenyl-4'-yl)nonane (CB9CB) and RM734 were synthesized in our laboratory [19,25]. Molecular structures and the phase transition temperatures are shown in Fig. [1(a)] and Fig. [1(c)], respectively. CB9CB molecules are bent shaped due to the flexible odd-numbered hydrocarbon link and RM734 molecules are wedged shaped because of the lateral methoxy
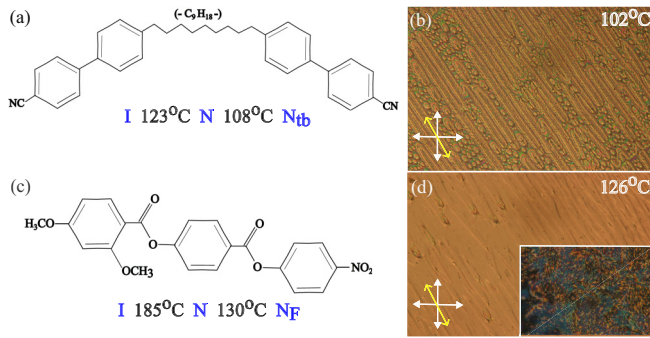

FIG. 1. (a) Molecular structures and phase transition temperatures of (a) CB9CB and (c) RM734 compounds. Textures of (b) N_{tb} and (d) N_F phases in planar cells (10 μm). The width of the image is 0.7 mm. Inset shows texture in an untreated cell.
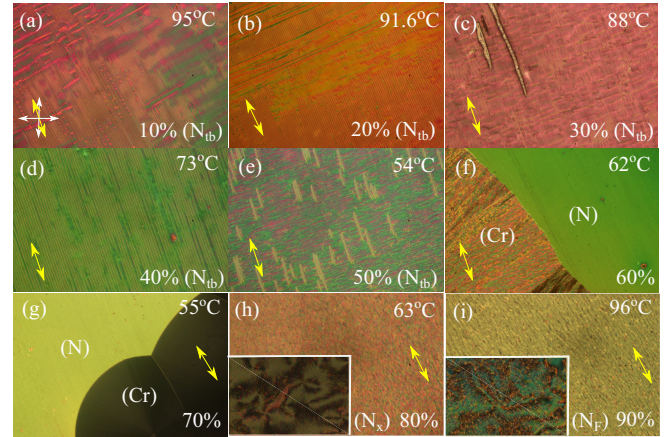

FIG. 2. Representative polarizing optical microscope (POM) textures of a few mixtures at different temperatures. Double-headed yellow arrows indicate the rubbing direction. Wt. % of RM734 and the temperatures are marked on each image. (a)–(e) N_{tb} phase, (f),(g) N to crystal transition, (h) N_x phase, and (i) N_F phase. Width of an image is 1.3 mm. Insets show textures in untreated cells.

group [34]. At room temperature both the compounds are in powder form. Appropriate weights of each material were put together in a conical glass cup and heated to 190 °C. The sample was mixed thoroughly by continuously stirring for several minutes.

Cells were made with indium-tin-oxide (ITO) coated glass plates of size 15 mm × 10 mm. Polyamides PI2555 (HD MicroSystems) and JALS 204 (JSR Corporation) were spin coated on the ITO plates to obtain planar (or homogeneous) and homeotropic alignment of the samples, respectively. The coated plates were cured at an appropriate temperature. To make planar cells, baked plates were machine rubbed unidirectionally and assembled like a parallel-plate capacitor. The cell gap was maintained by mixing transparent silica beads (≈10 μm) with UV curable glue. Planar cells were filled by the sample in the nematic phase. Textures of the samples were viewed using a polarizing optical microscope (NIKON POL100). The temperature of the sample was controlled using an Instec (HSC402) hot stage and MK2000 controller. The birefringence (Δn) measurement was carried out using a phase modulation technique [35,36]. The setup for the electro-optical measurements consists of a He-Ne laser ($\lambda = 632.8$ nm, Thorlabs), photoelastic modulator (HINDS PEM 100), a pair of crossed Glans-Thompson polarizers, photodetector (HINDS), multimeter (Keithley, 2000 series), and two lock-in amplifiers (Amtek SR7265 and Standford Research SR830). In this technique the polarization of the incident light is modulated at the frequency of 50 kHz and the first and the second harmonics of the transmitted intensity through the cell are measured by the photodetector and the lock-in amplifiers. The birefringence of the sample is given by [35,36]

$$\Delta n = \frac{\lambda}{2\pi d} \tan^{-1}\left(\frac{I_{1f} J_2(A_0)}{I_{2f} J_1(A_0)}\right), \tag{1}$$

where d is the cell thickness, λ is the wavelength of the light, I_{1f} and I_{2f} are the first and second harmonics optical signals measured by the lock-in amplifiers, J_1 and J_2 are the first and second order Bessel functions, and A_0 is the retardation of the PEM. The setup is capable of measuring optical retardation up to 0.1 nm [36]. For dielectric measurements, the ITO electrodes on each substrate were etched into a circular pattern with a diameter of about 7 mm. An LCR meter (E4980A,

Agilent) was used to measure the dielectric constant in the frequency range of 20 Hz to 2 MHz. The splay elastic constant (K_{11}) is calculated from the threshold voltage of the Freedericksz transition. The spontaneous polarization was measured by applying an in-plane ac electric field along the director following the procedure reported [15]. A brief description of the setup is provided in the Supplemental Material (Fig. S5) [37]. All the instruments were computer interfaced and appropriate LabView programs were developed to control the experiments.

III. RESULTS AND DISCUSSION

Phase transitions of all the compounds and their mixtures were studied using a polarizing optical microscope (POM) and a differential scanning calorimeter (Mettler Toledo DSC 3). Figures 1(b) and 1(d) show typical textures of N_{tb} (threadlike focal conics) and N_F phases (lens-shaped domains), respectively. Figures [2(a)–2(i)] show some representative textures of a few mixtures at different temperatures. Up to 50 wt. %, the low-lying nematic exhibit a typical texture of N_{tb} phase having elongated threadlike structures running parallel to the rubbing direction. No nematic to nematic transition is observed in the mixtures 60 wt. % and 70 wt. % [Figs. 2(f) and 2(g)]. In the mixtures, above 80 wt. %, again the nematic to nematic transition is observed and the low-lying nematic textures look like a typical N_F phase [e.g., Fig. 2(h)]. However, the low-temperature nematic phase for 85 and 80 wt. % is not polar; hence it is designated as N_x [Fig. 2(h); see later discussion]. In the mixture of 90 wt. % RM734 the low-lying nematic is ferroelectric [Fig. 2(i)].

Figure 3(a) presents the phase diagram of the mixtures of CB9CB and RM734 mesogens. The open symbols represent phase transition temperatures obtained from the texture change observed under a polarizing optical microscope. The filled symbols represent the phase transition temperatures obtained from the differential scanning calorimetry (DSC)
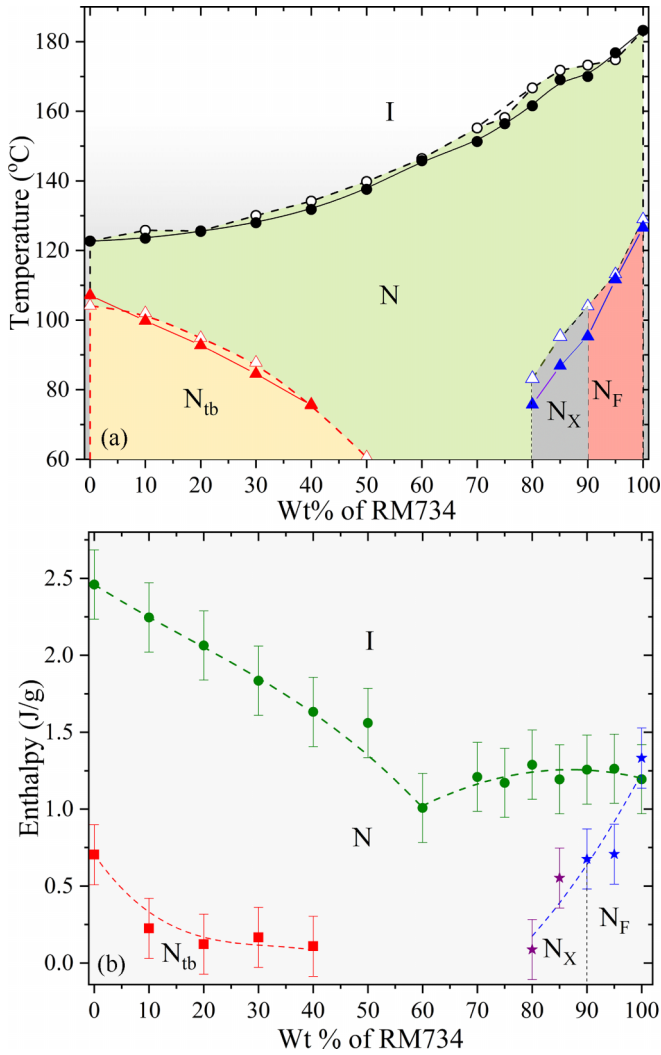
FIG. 3. (a) Phase diagrams of CB9CB and RM734 mixtures. Filled and open symbols represent transition temperatures obtained from DSC and POM, respectively. (b) Enthalpies of N-I transition (green circles), N-N_{tb} transition (red squares), and N-N_F or N-N_x transitions (stars). Dashed lines are drawn as a guide to the eye. Error bars represent the standard deviation of the mean. N_x denotes a nematic phase whose texture is similar to N_F without polarization.

studies. The DSC measurements were made at the cooling or heating rate of 5 °C/min, whereas POM studies were done at 1 °C/min. Nevertheless, the phase transition temperatures obtained from two different methods agree quite well.

The phase diagram can be divided into three regions. In the low concentration region of RM734 (0–50 wt. %), the nematic to isotropic (N-I) transition temperature increases, while the N-N_{tb} transition temperature decreases significantly. For example, at 50 wt. %, the N-N_{tb} phase transition temperature came down to about 60 °C compared to the N-N_{tb} phase transition temperature in pristine CB9CB (108 °C). In the high-concentration region (80–100 wt. %) the N-N_F or N-N_x phase transition temperature also decreases notably. For example, at 90 wt. % the N-N_F transition temperature is reduced by 30 °C. In the intermediate concentration region (~60–70 wt. %) no nematic to N_{tb} or N-N_F transitions are observed. It

is known that the shape and the flexibility of the hydrocarbon link of CB9CB molecules play a crucial role in stabilizing the N_{tb} phase. The addition of rigid rodlike molecules (RM734) might affect these factors and reduce the stability of the N_{tb} phase. On the other side of the phase diagram, a very small concentration of CB9CB greatly reduces the polar order and hence the stability of the N_F phase.

Figure 3(b) shows the variation of enthalpy of N-I, N-N_{tb}, and N-N_F phase transitions of the mixtures including pristine mesogens. The enthalpy of the N-I phase transition decreases with increasing concentration of RM734 (till 60 wt. %). The enthalpy of N-N_{tb} (0–40 wt. %) or N-N_F/N_x (80–100 wt. %) transitions also decreases substantially compared to the values of the pristine mesogens. For example, the enthalpy of the N-N_{tb} transition of pristine CB9CB is 0.75 J/g and it reduces to about 0.1 J/g when the concentration of RM734 is increased to 40 wt. %. For 50 wt. %, although a clear textural change is observed in the POM, no enthalpy associated with the N-N_{tb} transition could be detected in the DSC measurements. This suggests that the N-N_{tb} phase transition becomes second order at this concentration. The reduced temperature $T_{N_{tb}-N}/T_{NI}$ is related to the nature of the phase transition [38], similar to the McMillan ratio in the case of N-SmA transition. It decreases from 0.96 to about 0.86 (40 wt. %) and is consistent with the decreasing enthalpy of the transition. A similar reduction of enthalpy was reported in the binary mixtures of CB9CB and 5CB (pentyl cyanobiphenyl) [39] and FFO9OCB compounds [40]. In 60 wt. % and 70 wt. % mixtures, the nematic (N) to crystal phase transition occurs below 60 °C [not shown in Fig. 3(b)]. Similarly the enthalpy of the N-N_F transition of the pristine RM734 mesogen is 1.2 J/g and it decreases very rapidly to about 0.25 J/g when the concentration is reduced to 80 wt. %. It may be noted that there is no biphasic region in the phase diagram. This is perhaps due to the same macroscopic symmetry of both phases.

We have theoretically calculated the eutectic composition and phase transition temperatures (melting and clearing points). We used CSL equations (Le Chatelier–Schröder–van Laar) [41–44] for predicting the eutectic melting temperature of the mixtures and Cox and Johnson equations for clearing temperature [41–44]. The CSL equations for a two-component mixture are given by

$$\ln(x_i) = \frac{\Delta H}{R}\left(\frac{1}{T_i} - \frac{1}{T}\right), \qquad (2)$$

where T_i is the melting temperature and R is the molar gas constant. The melting enthalpies and melting points for RM734 and CB9CB are taken from the DSC data and are given by $\Delta H_m^{RM734} = 32868$ J/mol, $T_m^{RM734} = 141.7$ °C and $\Delta H_m^{CB9CB} = 35806$ J/mol, $T_m^{CB9CB} = 82.5.7$ °C, respectively. Taking the compositions in molar fractions $x_{RM734} = 0.185$ and $x_{CB9CB} = 0.815$, the calculated melting and clearing temperatures of the eutectic point are $T_m = 79.2$ °C and 134.4 °C, respectively. The corresponding eutectic composition (in wt. %) is composed of 83.5 wt. % CB9CB and 16.5 wt. % RM734. This composition does not match with the composition at which the enthalpy of the NI transition drops suddenly (60 wt. % RM734). Hence the enthalpy drop may be associated with the poor miscibility of the polar phase. We measured the spontaneous polarization (P_S) of the pristine
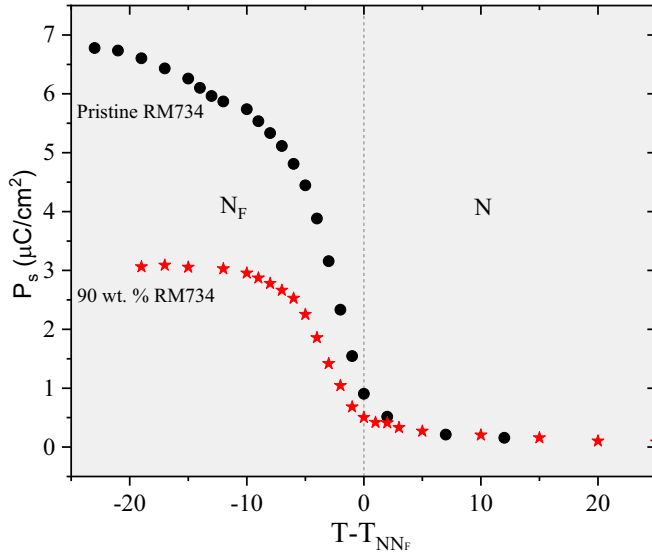
FIG. 4. Temperature dependent spontaneous polarization (P_S) for pristine RM734 and 90 wt. % mixture.

RM734 and a mixture (Fig. 4). The diagram of the experimental setup is presented in the Supplemental Material (Fig. S4) [37]. The spontaneous polarization increases with decreasing temperature as expected and the temperature dependence of P_S of pristine RM734 also agrees well with the values reported by Chen *et al.* [15]. In the mixture (90 wt. %) the polarization decreases significantly. For example, the polarization of the pristine RM734 at a shifted temperature $T - T_{\text{N-N}_F} = -10\,^\circ\text{C}$ is $P_S \sim 6\ \mu\text{C/cm}^2$ and it reduced to about $\sim 3\ \mu\text{C/cm}^2$ of the mixture. However, no polarization peak was observed for 85 and 80 wt. % mixtures. Hence, in these two mixtures, the low-lying nematic phase is assigned as N_x, which could be a superparaelectric phase. We have not further characterized this phase.

As a next step, we measured the temperature-dependent birefringence (Δn) of the mixtures. Figure 5(a) shows the variation of Δn of a few mixtures and the pristine mesogens. All the samples show a discontinuous jump in Δn corresponding to the first-order N-I phase transition followed by a gradual increase with decreasing temperature. An abrupt decrease in Δn at different temperatures of the mixtures (0–50 wt. %) indicates the onset of the N-N$_{tb}$ phase transition. The temperature-dependent birefringence above the N-N$_{tb}$ transition can be fitted to the Haller formula [45]

$$\Delta n_p = \Delta n_{\text{max}}(1 - T/T^*)^\beta, \qquad (3)$$

where Δn_{max} is the birefringence of the perfectly aligned nematic phase when the orientational order parameter $S = 1$ and β is the critical exponent connected to the N-I phase transition. A representative fit of Δn to Eq. (1) for 10 wt. % is shown in the inset of Fig. 5(a). The exponent obtained for different samples is about 0.2. As the N-N$_{tb}$ transition is approached from the high-temperature N phase, the measured birefringence deviates from the prediction of the Haller extrapolation. This deviation is an indication of pretransitional tilt fluctuations of the director due to the formation of local helical structures in the N-N$_{tb}$ transition [46]. The fluctuation
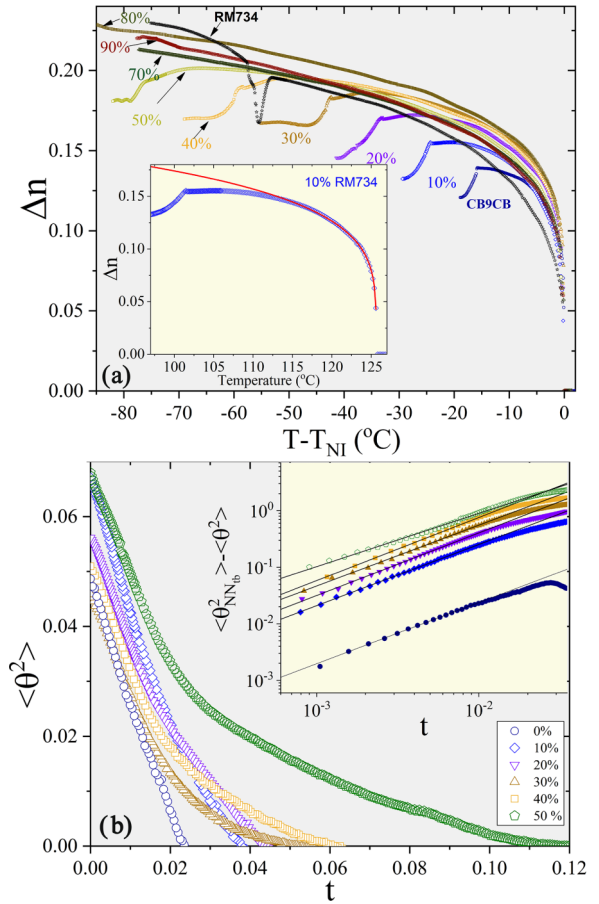

FIG. 5. (a) Variation of birefringence Δn with shifted temperature with increasing wt. % of RM734. Inset shows the variation of Δn together with the Haller fit (red line) for 10 wt. % of RM734. (b) Mean-square fluctuations $\langle \theta^2 \rangle$ of the heliconical tilt angle calculated from Eq. (2). Inset shows temperature variation of relative tilt fluctuations $\langle \theta^2_{NN_{tb}} \rangle - \langle \theta^2 \rangle \sim t^{1-\alpha}$ with $1 - \alpha$ close to 1. For clarity, the critical components of fluctuations are shifted by multiples of 10 along the Y axis. Cell thickness is 9.4 μm.

is evident up to 50 wt. % of the mixture. The mean-square tilt angle fluctuations $\langle \theta^2 \rangle$ can be obtained approximately using the following equation [47]:

$$\Delta n_p(T) = \Delta n_0\left(1 - \tfrac{3}{2}\langle \theta^2 \rangle\right), \qquad (4)$$

where Δn_p is the measured value and Δn_0 is obtained from the extrapolated birefringence [see Eq. (3)] in the absence of fluctuations. Figure 5(b) shows variation of $\langle \theta^2 \rangle$ as a function of reduced temperature $t = \frac{T - T_{NN_{tb}}}{T_{NN_{tb}}}$, where $T_{NN_{tb}}$ is the N to N$_{tb}$ phase transition temperature. The critical component of the fluctuation depends on temperature and is theoretically predicted to vary as [47]

$$\langle \theta^2_{NN_{tb}} \rangle - \langle \theta^2 \rangle \sim t^{1-\alpha}, \qquad \text{for} \quad t > 0 \qquad (5)$$

where $\langle \theta^2_{NN_{tb}} \rangle$ and α are maximum fluctuations at the transition and the exponent of the heat capacity, respectively. The inset of Fig. 5(b) shows the variation of $\langle \theta^2_{NN_{tb}} \rangle - \langle \theta^2 \rangle$ with t. Table I shows that $1 - \alpha$ is closer to 1 for all the samples which means there should not be any heat capacity anomalies

TABLE I. Critical exponents obtained from different mixtures.

Wt. % of RM734 in the mixtures	$1-\alpha$ (± 0.02)
0 wt. %	1.08
10 wt. %	1.08
20 wt. %	1.1
30 wt. %	1.07
40 wt. %	1.1
50 wt. %	0.95

above the transition temperature. Similar critical behavior of the birefringence was reported in CB7CB and other twist-bend liquid crystals exhibiting a broad temperature range of the nematic phase [46]. The temperature range of the apolar nematic (N) phase increases with increasing wt. % of RM734. Consequently, the critical range of tilt fluctuations increases. This is expected as the fluctuations should be stronger for

the mixtures having a wider nematic range above the N-N_{tb} phase transition temperature [38,48]. The strength of the first-order phase transition is related to the effective twist elastic constant (K_2^{eff}) [38]. In the mixture, with increasing wt. % of RM734, the first-order transition becomes progressively weaker and eventually becomes second order. Hence the temperature range and strength of the fluctuations suggest that the twist elastic constant in the mixture decreases significantly.

In what follows we measure the splay elastic constant of the high-temperature nematic phase from the Freedericksz transition. We used an electro-optical method and measured the optical retardation of a planar cell as a function of the applied voltage perpendicular to the director. The frequency of the voltage was selected which is far away from both low and high frequency dielectric relaxation regions. The Freedericksz threshold voltage was obtained at which the birefringence starts decreasing rapidly. Some representative voltage-dependent birefringence curves are shown in the
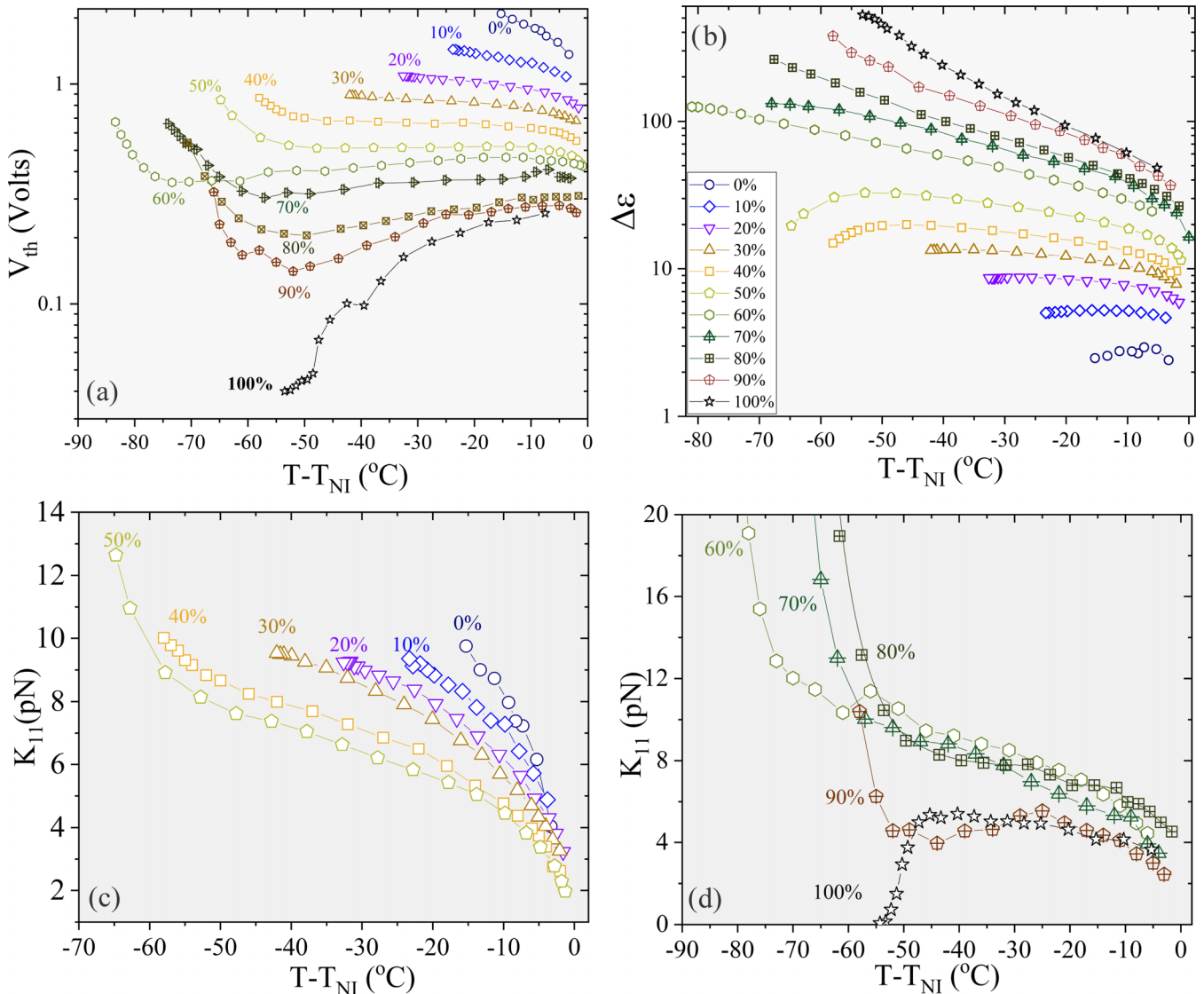

FIG. 6. Temperature (shifted) dependence of (a) Freedericksz threshold voltage V_{th}, (b) dielectric anisotropy ($\Delta\epsilon$), and (c),(d) splay elastic constant K_{11} at different wt. % of RM734. For clarity of different mixtures K_{11} is shown in two different plots. Cell thickness is 10.5 μm.

Supplemental Material (Fig. S1) [37]. Figure 6(a) shows the variation of Freedericksz threshold voltage as a function of shifted temperature. V_{th} of pristine CB9CB is much larger than that of pristine RM734. At any fixed temperature V_{th} decreases gradually as the wt. % of RM734 in the mixture increases. Up to 30 wt. %, V_{th} increases with decreasing temperature as $V_{th} \propto S$, where S is the orientational order parameter which increases with decreasing temperature from the N-I transition. The curvature of the temperature-dependent V_{th} changes above 40 wt. % of RM734. For example, it tends to diverge at lower temperatures in 40–50 wt. % mixtures. Between 60 to 90 wt. %, V_{th} shows a minimum and at 90 wt. % it reaches to a very small value. Estimation of splay elastic constant from V_{th} requires dielectric anisotropy $\Delta\epsilon$ ($= \epsilon_{\parallel} - \epsilon_{\perp}$). Above 50 wt. % of RM734, $\epsilon_{\perp}$ and $\epsilon_{\parallel}$ were measured in planar and homeotropic cells, respectively. This method cannot be used for mixtures below 60 wt. % as the homeotropic alignment of the sample is not uniform. Hence we measured the voltage-dependent dielectric constant in a planar cell and $\epsilon_{\parallel}$ was obtained from the extrapolation of the high-voltage data (see Fig. S3 of the Supplemental Material [37]) [30,49]. The dielectric properties of RM734 are quite complex and also depend on the measuring cell thickness [50–53]. We kept the cell thickness almost fixed ($\simeq$10 μm) for all dielectric measurements. For each sample, we performed dielectric dispersion studies and selected the dielectric constant in an appropriate frequency that is away from any dielectric relaxation. Some representative dielectric relaxation dispersion curves are presented in the Supplemental Material [37] (see Fig. S2).

Figure 6(b) shows the variation of $\Delta\epsilon$ for all the samples as a function of shifted temperature. In pristine CB9CB, the anisotropy is small and positive. It increases with increasing concentration of RM734 as expected because molecules of RM734 mesogen have a very large axial dipole moment ($\approx$11 D). In pristine RM734, the anisotropy is very high [14]. It can be noted that the temperature dependence of $\Delta\epsilon$ below 50 wt. % is noticeably different than the higher concentrations. For example, above 50 wt. %, $\Delta\epsilon$ increases very rapidly with decreasing temperature and does not follow the usual trends of the order parameter (i.e., $\Delta\epsilon \propto S$). This response can be attributed to the presence of pretransitional polar domains [25]. Below 50 wt. % the curvature of the temperature-dependent anisotropy is different. In particular, it reaches a maximum at some intermediate temperature and decreases as the temperature is lowered towards the N-N$_{tb}$ phase transition temperature and deviates from the power-law dependence (see Fig. S4 of the Supplemental Material [37]). Such deviation in $\Delta\epsilon$ is consistent with the pretransitional birefringence fluctuations discussed in the previous section. Similar behavior was observed in other N$_{tb}$ mesogens [46].

The splay elastic constant K_{11} was calculated directly using the relation $K_{11} = \frac{V_{th}^2 \epsilon_o \Delta\epsilon}{\pi^2}$ [54]. Figures 6(c) and 6(d) show the variation of K_{11} with shifted temperature. The temperature dependence of K_{11} of pristine CB9CB agrees well with measurements reported previously [48,55]. Below 30 wt. %, the mixtures show a usual temperature dependence, i.e., K_{11} increases with decreasing temperature ($K_{11} \propto S^2$) [Fig. 6(c)]. Above 30 wt. %, K_{11} changes curvature and diverges as the

temperature is reduced. For example, K_{11} in the range of mixtures 50–80 wt. %, shows a steep rise as the nematic to low-temperature nematic transition is approached. Similar results have been reported in a few bent-core compounds which do not follow the mean field dependence [49,56]. Recently, a very unusual increase of splay elastic constant from nematic to twist bend nematic has been reported in thioether-based twist bend nematic liquid crystal [57]. It has been shown that compounds having nematic to the low-lying higher-order phase pretransitional behavior of the elastic constants can be explained well due to third-order dependency on the order parameter as proposed by Berreman and Meiboom [58,59]. In the present system, the orientational order of the low-lying phases (N$_F$, N$_x$, and crystal) is higher and this could be responsible for the observed pretransitional divergence. The temperature dependence of K_{11} for pure RM734 is the opposite, i.e., it decreases sharply as the N-N$_F$ transition is approached. Such a decrease is proposed to originate from the strong splay fluctuations [12]. The temperature dependence of the splay elastic constant of 90 wt. % is very unusual—namely, it shows a minimum. This behavior could be attributed to the two competing effects. As the temperature is reduced towards the N-N$_F$ transition, the moderate splay fluctuations (comparatively smaller than the pristine RM734) tend to reduce K_{11}. On the other hand, as the temperature decreases the influence of third-order dependency due to the low-lying higher-order phase begins. As a result of these two effects, the splay elastic constant could show a minimum just before the phase transition. However, further studies, such as atomistic calculations of the elastic constants, could shed more light on this result.

IV. CONCLUSION

We studied the binary phase diagram of RM734 and CB9CB mesogens. In the mixtures, N-N$_{tb}$ and N-N$_F$ phase transition temperatures decrease substantially compared to the pristine mesogens and, eventually, these two transitions disappear at some intermediate concentrations stabilizing only apolar nematic phase. The enthalpy of both N-N$_{tb}$ and N-N$_F$ transitions in the mixtures also decreases, suggesting these weak first-order transitions become weaker and such a response is consistent with the decrease of the reduced temperature N$_{tb-N}$/T$_{NI}$ as predicted in the theory. At about 50 wt. % of RM734, the N-N$_{tb}$ phase transition becomes second order. From 60 wt. % to 70 wt. % of RM734, neither N-N$_{tb}$ nor N-N$_F$ phase transitions are observed. The temperature range of the critical birefringence fluctuations, reflecting the twist fluctuations, is widened with increasing concentration of RM734, although the critical exponent $1 - \alpha$ in the mixtures remains unaffected. The tilt fluctuations are also evident in the temperature-dependent dielectric anisotropy. The temperature dependence of the splay elastic constant at higher concentrations (50–90 wt. %) of RM734 is significantly different than that of the pristine mesogens. In the low concentration range of RM734 the splay elastic constant follows the prediction of the mean field. In the intermediate range, the effect of low-lying higher order phase is evident and, in the pristine

RM734, the splay fluctuations dominate. A small addition of CB9CB in pristine RM734 remarkably reduces the polar interaction and hence the spontaneous polarization. Our results suggest that despite their macroscopic resemblance (both being nematic) these two mesogens are incompatible for mixing due to structural disparity. These results may invoke further studies on ferroelectric nematic-based mixtures for rich phase diagrams and new physical properties.

[1] V. P. Panov, M. Nagaraj, J. K. Vij, Yu. P. Panarin, A. Kohlmeier, M. G. Tamba, R. A. Lewis, and G. H. Mehl, Phys. Rev. Lett. **105**, 167801 (2010).

[2] M. Cestari, E. Frezza, A. Ferrarini, and G. R. Luckhurst, J. Mater. Chem. **21**, 12303 (2011).

[3] M. Cestari, S. Diez-Berart, D. A. Dunmur, A. Ferrarini, M. R. de la Fuente, D. J. B. Jackson, D. O. Lopez, G. R. Luckhurst, M. A. Perez-Jubindo, R. M. Richardson, J. Salud, B. A. Timimi, and H. Zimmermann, Phys. Rev. E **84**, 031704 (2011).

[4] D. Chen, J. H. Porada, J. B. Hooper, A. Klittnick, Y. Shena, M. R. Tuchbanda, E. Korblova, D. Bedrov, D. M. Walba, M. A. Glaser, J. E. Maclennana, and N. A. Clark, Proc. Natl. Acad. Sci. USA **110**, 15931 (2013).

[5] M. Čopič, Proc. Natl. Acad. Sci. USA **110**, 15855 (2013).

[6] V. Borshch, Y. K. Kim, J. Xiang, M. Gao, A. Jakli, V. P. Panov, J. K. Vij, C. T. Imrie, M. G. Tamba, G. H. Mehl, and O. D. Lavrentovich, Nat. Commun. **4**, 2635 (2013).

[7] L. Beguin, J. W. Emsley, M. Lelli, A. Lesage, G. R. Luckhurst, B. A. Timimi, and H. Zimmermann, J. Phys. Chem. B **116**, 7940 (2012).

[8] G. Pająk, L. Longa, and A. Chrzanowska, Proc. Natl. Acad. Sci. USA **115**, E10303 (2018).

[9] R. J. Mandle, S. J. Cowling, and J. W. Goodby, Chem. A Eur. J. **23**, 14554 (2017).

[10] R. J. Mandle and A. Mertelj, Phys. Chem. Chem. Phys. **21**, 18769 (2019).

[11] H. Nishikawa, K. Shiroshita, H. Higuchi, Y. Okumura, Y. Haseba, S.-I. Yamamoto, K. Sago, and H. Kikuchi, Adv. Mater. **29**, 1702354 (2017).

[12] A. Mertelj, L. Cmok, N. Sebastián, R. J. Mandle, R. R. Parker, A. C. Whitwood, J. W. Goodby, and M. Čopič, Phys. Rev. X **8**, 041025 (2018).

[13] A. Manabe, M. Bremer, and M. Kraska, Liq. Cryst. **48**, 1079 (2021).

[14] N. Sebastián, L. Cmok, R. J. Mandle, M. R. de la Fuente, I. Drevenseck Olenik, M. Čopič, and A. Mertelj, Phys. Rev. Lett. **124**, 037801 (2020).

[15] X. Chen, E. Korblova, D. Dong, X. Wei, R. Shao, L. Radzihovsky, M. A. Glaser, J. E. Maclennan, D. Bedrov, D. M. Walba, and N. A. Clark, Proc. Natl. Acad. Sci. USA **117**, 14021 (2020).

[16] M. Born, Sitzungsber. K. Preuss. Akad. Wiss. **30**, 614 (1916).

[17] I. Dozov, Europhys. Lett. **56**, 247 (2001).

[18] M. P. Kumar, P. Kula, and S. Dhara, Phys. Rev. Mater. **4**, 115601 (2020).

[19] M. P. Kumar, J. Karcz, P. Kula, and S. Dhara, Phys. Rev. Mater. **5**, 115605 (2021).

[20] Z. Parsouzi, S. A. Pardaev, C. Welch, Z. Ahmed, G. H. Mehl, A. R. Baldwin, J. T. Gleeson, O. D. Lavrentovich, D. W. Allender, J. V. Selinger, A. Jakli, and S. Sprunt, Phys. Chem. Chem. Phys. **18**, 31645 (2016).

[21] A. Barthakur, J. Karcz, P. Kula, and S. Dhara, Phys. Rev. Mater. **7**, 035603 (2023).

[22] M. T. Máthé, Á. Buka, A. Jákli, and P. Salamon, Phys. Rev. E **105**, L052701 (2022).

[23] R. Barboza, S. Marni, F. Ciciulla, F. A. Mir, G. Nava, F. Caimi, A. Zaltron, N. A. Clark, T. Bellini, and L. Lucchetti, Proc. Natl. Acad. Sci. USA **119**, e2207858119 (2022).

[24] M. T. Máthé, B. Farkas, L. Péter, Á. Buka, A. Jákli, and P. Salamon, Sci. Rep. **13**, 6981 (2023).

[25] M. P. Kumar, J. Karcz, P. Kula, S. Karmakar, and S. Dhara, Phys. Rev. Appl. **19**, 044082 (2023).

[26] P. Kumari, B. Basnet, H. Wang, and O. D. Lavrentovich, Nat. Commun. **14**, 748 (2023).

[27] N. Sebastián, M. Lovšin, B. Berteloot, N. Osterman, A. Petelin, R. J. Mandle, S. Aya, M. Huang, I. Drevenšek-Olenik, K. Neyts, and A. Mertelj, Nat. Commun. **14**, 3029 (2023).

[28] F. Caimi, G. Nava, S. Fuschetto, L. Lucchetti, P. Paié, R. Osellame, X. Chen, N. A. Clark, M. A. Glaser, and T. Bellini, Nat. Phys. **19**, 1658 (2023).

[29] R. Pratibha, N. V. Madhusudana, and B. K. Sadashiva, Science **288**, 2184 (2000).

[30] B. Kundu, R. Pratibha, and N. V. Madhusudana, Phys. Rev. Lett. **99**, 247802 (2007).

[31] X. Chen, Z. Zhu, M. J. Magrini, E. Korblova, C. S. Park, M. A. Glaser, J. E. Maclennan, D. M. Walba, and N. A. Clark, Liq. Cryst. **49**, 1531 (2022).

[32] J. Zhou, R. Xia, M. Huang, and S. Aya, J. Mater. Chem. C **10**, 8762 (2022).

[33] H. Long, J. Li, M. Huang, and S. Aya, Liq. Cryst. **49**, 2121 (2022).

[34] N. Sebastian, R. J. Mandle, A. Petelin, A. Eremin, and A. Mertelj, Liq. Cryst. **48**, 2055 (2021).

[35] T. C. Oakberg, Proc. SPIE **3121**, 19 (1997).

[36] T. C. Oakberg, Proc. SPIE **2873**, 17 (1996).

[37] See Supplemental Material at http://link.aps.org/supplemental/10.1103/PhysRevE.109.024702 for additional information on threshold voltage, dielectric dispersion and polarization measurements.

[38] D. A. Paterson, M. Gao, Y.-K. Kim, A. Jamali, K. L. Finley, B. Robles-Hernández, S. Diez-Berart, J. Salud, M. R. de la Fuente, B. A. Timimi, H. Zimmermann, C. Greco, A. Ferrarini, J. M. D. Storey, D. O. López, O. D. Lavrentovich, G. R. Luckhurst, and C. T. Imrie, Soft Matter **12**, 6827 (2016).

[39] C. S. P. Tripathi, P. Losada-Perez, C. Glorieux, A. Kohlmeier, M. G. Tamba, G. H. Mehl, and J. Leys, Phys. Rev. E **84**, 041707 (2011).

[40] D. O. López, B. Robles-Hernández, J. Salud, M. R. de la Fuente, N. Sebastián, S. Diez-Berart, X. Jaen, D. A. Dunmurd, and G. R. Luckhurst, Phys. Chem. Chem. Phys. **18**, 4394 (2016).

[41] H. Le Chatelier, C. R. Acad. Sci. **100**, 50 (1885).

[42] I. Z. Schröder, J. Phys. Chem. **11**, 449 (1893).

[43] J. J. van Laar, Z. Phys. Chem. **63U**, 216 (1908).

[44] R. J. Cox and J. F. Johnson, IBM J. Res. Dev. **22**, 51 (1978).

[45] I. Haller, Prog. Solid State Chem. **10**, 103 (1975).

[46] D. Pociecha, C. A. Crawford, D. A. Paterson, J. M. D. Storey, C. T. Imrie, N. Vaupotič, and E. Gorecka, Phys. Rev. E **98**, 052706 (2018).

[47] K. C. Lim and J. T. Ho, Phys. Rev. Lett. **40**, 1576 (1978).

[48] B. Robles-Hernandez, N. Sebastian, M. R. de la Fuente, D. O. Lopez, S. Diez-Berart, J. Salud, M. B. Ros, D. A. Dunmur, G. R. Luckhurst, and B. A. Timimi, Phys. Rev. E **92**, 062505 (2015).

[49] P. Sathyanarayana, B. K. Sadashiva, and S. Dhara, Soft Matter **7**, 8556 (2011).

[50] N. Vaupotič, D. Pociecha, P. Rybak, J. Matraszek, M. Čepič, J. M. Wolska, and E. Gorecka, Liq. Cryst. **50**, 584 (2023).

[51] N. A. Clark, X. Chen, J. E. Maclennan, and M. A. Glaser, arXiv:2208.09784.

[52] R. J. Mandle, N. Sebastián, J. Martinez-Perdiguero, and A. Mertelj, Nat. Commun. **12**, 4962 (2021).

[53] A. Erkoreka, J. Martinez-Perdiguero, R. J. Mandle, A. Mertelj, and N. Sebastián, J. Mol. Liq. **387**, 122566 (2023).

[54] P. G. de Gennes, *The Physics of Liquid Crystals* (Oxford University Press, Oxford, England, 1974).

[55] M. Čopič and A. Mertelj, Phys. Rev. E **101**, 022704 (2020).

[56] P. Sathyanarayana, M. C. Varia, A. K. Prajapati, B. Kundu, V. S. S. Sastry, and S. Dhara, Phys. Rev. E **82**, 050701(R) (2010).

[57] J. Zhou, W. Tang, Y. Arakawa, H. Tsujib, and S. Aya, Phys. Chem. Chem. Phys. **22**, 9593 (2020).

[58] D. W. Berreman and S. Meiboom, Phys. Rev. A **30**, 1955 (1984).

[59] S. Kaur, H. Liu, J. Addis, C. Greco, A. Ferrarini, V. Gortz, J. W. Goodby, and H. F. Gleeson, J. Mater. Chem. C **1**, 6667 (2013).